Acta Crystallographica Section F
Structural Biology and Crystallization Communications
ISSN 1744-3091

Overexpression, purification, crystallization and preliminary structural studies of catabolic ornithine transcarbamylase from *Lactobacillus hilgardii*

Blanca de las Rivas,[a] Héctor Rodríguez,[a] Iván Angulo,[b] Rosario Muñoz[a] and José M. Mancheño[b]*

[a]Instituto de Fermentaciones Industriales, CSIC, Juan de la Cierva 3, 28006 Madrid, Spain, and [b]Grupo de Cristalografía Macromolecular y Biología Estructural, Instituto Rocasolano, CSIC, Serrano 119, 28006 Madrid, Spain

Correspondence e-mail: xjosemi@iqfr.csic.es

Received 27 March 2007
Accepted 23 May 2007

The catabolic ornithine transcarbamylase (cOTC; EC 2.1.3.3) from the lactic acid bacteria *Lactobacillus hilgardii* is a key protein involved in the degradation of arginine during malolactic fermentation. cOTC containing an N-terminal His_6 tag has been overexpressed in *Escherichia coli*, purified and crystallized under two different experimental conditions using the hanging-drop vapour-diffusion method. Crystals obtained from a solution containing 8%(*w*/*v*) PEG 4000, 75 m*M* sodium acetate pH 4.6 belong to the trigonal space group *P*321 and have unit-cell parameters $a = b = 157.04$, $c = 79.28$ Å. Conversely, crystals grown in 20%(*v*/*v*) 2-methyl-2,4-pentanediol, 7.5%(*w*/*v*) PEG 4000, 100 m*M* HEPES pH 7.8 belong to the monoclinic space group *C*2 and have unit-cell parameters $a = 80.06$, $b = 148.90$, $c = 91.67$ Å, $\beta = 100.25^\circ$. Diffraction data were collected in-house to 3.00 and 2.91 Å resolution for trigonal and monoclinic crystals, respectively. The estimated Matthews coefficient for the crystal forms were 2.36 and 2.24 $Å^3$ Da^{-1}, respectively, corresponding to 48% and 45% solvent content. In both cases, the results are consistent with the presence of three protein subunits in the asymmetric unit. The structure of cOTC has been determined by the molecular-replacement method using the atomic coordinates of cOTC from *Pseudomonas aeruginosa* (PDB code 1dxh) as the search model.

1. Introduction

Malolactic fermentation (MLF), which occurs after alcoholic fermentation during wine making, is induced by the growth of lactic acid bacteria (LAB; Liu & Pilone, 1998). MLF involves the decarboxylation of L-malic acid to L-lactic acid and carbon dioxide, which has important and desirable oenological consequences: the deacidification of acid wines, the addition of flavour to wines and increased microbial stability (Davis *et al.*, 1985). In addition, a key process accomplished by some LAB during MLF, also with great impact on oenology, involves the catabolism of the amino-acid arginine (Liu & Pilone, 1998), one of the main amino acids found not only in grape juice (Spayd & Andersen-Bagge, 1996) but also in wine (Lehtonen, 1996). Although the pathway of arginine degradation in wine LAB has been controversial until recently (arginase-urease *versus* arginine deiminase; Liu & Pilone, 1998), the arginine deiminase (ADI) pathway has been confirmed to be present in wine LAB that are able to catabolize this amino acid (Liu *et al.*, 1995; Arena *et al.*, 1999). This pathway includes three enzymes: ADI (EC 3.5.3.6), catabolic ornithine transcarbamylase (cOTC; EC 2.1.3.3) and carbamate kinase (CK; EC 2.7.2.2). According to the reaction scheme, one mole of arginine is converted into two moles of ammonia and one mole each of ornithine, ATP and carbon dioxide. This catabolic pathway has been suggested to provide the organisms not only with a source of energy that can be coupled to cellular growth, but also with a strategy for biological adaptation to the acid environment of wine (Liu & Pilone, 1998). In this sense, the production of ammonia may be physiologically relevant owing to its buffering capacity.

The metabolism of arginine by wine LAB during MLF has additional oenological implications which are related to the formation of ethyl carbamate (ETC) precursors. ETC is a human carcinogen (Mirvish, 1968) that is present in wines (Ough, 1993) and the

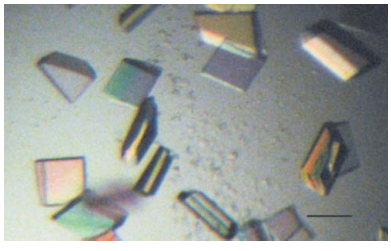

concentration of which is controlled (Canas *et al.*, 1994). The formation of ETC proceeds spontaneously and involves ethanol and precursors including urea, citrulline and carbamyl phosphate (Ough *et al.*, 1998). Even though the main source of ETC precursors is derived from arginine metabolism by yeasts (Monteiro & Bisson, 1991), a good correlation has been demonstrated between citrulline production and ETC formation during MLF (Sponholz, 1991, 1992). Thus, wine LAB have the potential to contribute to ETC formation as a consequence of the activity and regulation of the enzymes participating in the ADI pathway. In this sense, cOTC, the enzyme directly responsible for citrulline production, is of particular interest and may be suggested to be a key element in the process of modulation of ETC formation.

The three-dimensional structures of several OTCs have been reported: catabolic *Pseudomonas aeruginosa* OTC (Villeret *et al.*, 1995; PDB codes 1ort and 1dxh), anabolic *Escherichia coli* OTC (Jin *et al.*, 1997, PDB code 1akm; Ha *et al.*, 1997, PDB code 2otc), anabolic *Pyrococcus furiosus* OTC (Villeret *et al.*, 1998, PDB code 1a1s; Massant *et al.*, 2003, PDB code 1pvv) and human OTC (Shi *et al.*, 1998; PDB code 1oth). Comparative structural analysis revealed that most OTCases are homotrimeric, with the exception of cOTC from *P. aeruginosa* (Villeret *et al.*, 1995) and anabolic OTC from *P. furiosus* (Villeret *et al.*, 1998), which are dodecameric structures built up of four homotrimers. In all cases, the tertiary structure of the individual subunits is highly conserved and similar to those found in other transcarbamoylases (Lipscomb, 1994; Tuchman *et al.*, 1995).

In this work, we report the cloning of the *arcB* gene from *L. hilgardii* and the overexpression, purification, crystallization and preliminary X-ray crystallographic analysis of the catabolic ornithine transcarbamylase. Moreover, the crystal structure of cOTC has been solved by the molecular-replacement method using the atomic coordinates of catabolic ornithine transcarbamylase from *Pseudomonas aeruginosa* (Villeret *et al.*, 1995; PDB code 1dxh) as the search model.

2. Materials and methods

2.1. Cloning and overexpression

The *arcB* gene (coding for ornithine transcarbamylase; EC 2.1.3.3) from *L. hilgardii* CECT 4786^{T} (ATCC 8290^{T}) was PCR amplified by Hot-start Turbo *Pfu* DNA polymerase using primers 282 (5′-*CATCATGGTGACGATGACGATAAG*atgacaaaagattttagacaaaacg) and reverse 283 (5′-*AAGCTTAGTTAGCTATTATGCGTA*ctaggaatgaataggttacccaaag) (the nucleotides pairing the expression-vector sequence are indicated in italics and the nucleotides pairing the *arcB* gene sequence are indicated in lower case). The 1.0 kbp purified PCR product was inserted into pURI3 vector using the restriction-enzyme-free and ligation-free cloning strategy described by Geiser *et al.* (2001). Expression vector pURI3 was constructed based on the commercial expression vector pT7-7 (USB) but containing the leader sequence MGGSHHHHHHGDDDDKM consisting of an N-terminal methionine followed by three spacer amino acids, a six-histidine affinity tag, a spacer glycine residue and the five-amino-acid enterokinase recognition site (unpublished results). Thus, the final recombinant cOTC would possess 359 amino-acid residues with a molecular weight of 40 kDa. *E. coli* DH5α cells were transformed, recombinant plasmids were isolated and those containing the correct insert were identified by restriction-enzyme analysis, verified by DNA sequencing and then transformed into *E. coli* JM109(DE3) (pLysS) cells.

Cells carrying the recombinant plasmid pURI3-OTC were grown at 310 K in Luria–Bertani media containing ampicillin (100 µg ml^{-1}) and chloramphenicol (34 µg ml^{-1}) until they reached an optical density at 600 nm of 0.4 and were induced by adding 0.4 m*M* IPTG. After induction, the cells were grown at 295 K for 20 h and collected by centrifugation.

2.2. Purification

Cells were resuspended in 25 ml 20 m*M* Tris–HCl pH 8.0 containing 100 m*M* NaCl and disrupted using a French press. The lysate was centrifuged in an SS34 rotor at 20 000 rev min^{-1} for 30 min at 277 K using a Sorvall centrifuge. After filtration through a 0.45 µm filter (Millipore), the supernatant was loaded onto a His-Trap FF nickel-affinity column (GE Healthcare). The recombinant His_6-tagged protein was eluted with a 10–500 m*M* imidazole gradient using an AKTA Prime system (GE Healthcare). Fractions containing His_6-tagged cOTC were pooled and dialysed overnight at 277 K against 10 m*M* Tris–HCl pH 8.0 containing 10 m*M* NaCl. The protein solution was then loaded onto a HiTrap Q HP column (GE Healthcare) and elution was performed with a 10–500 m*M* NaCl gradient. Pooled fractions containing cOTC were dialysed overnight at 277 K against 10 m*M* Tris–HCl pH 8.0 containing 100 m*M* NaCl and further concentrated by ultrafiltration with YM-10 membranes (Amicon). A final chromatographic step was carried out on Superdex 200 prep grade (GE Healthcare) with a BioRad BioLogic DuoFlow FPLC. The elution profile indicated that cOTC behaves as an oligomeric species in solution with a molecular weight corresponding to a hexamer. Fractions containing cOTC were pooled and concentrated by ultrafiltration with YM-10 membranes (Amicon). Protein purity was checked by SDS–PAGE at various stages of the purification process (Fig. 1). The cOTC solution used for crystallization was finally prepared in 10 m*M* Tris–HCl pH 8.0 containing 100 m*M* NaCl. Protein concentration was determined by UV–Vis absorbance measurements with a Nanodrop ND-1000 spectrophotometer using an extinction coefficient of 0.885 (1 mg ml^{-1}, 1 cm, 280 nm).

2.3. Crystallization

Initial screening for crystallization conditions was carried out at 291 K by the hanging-drop vapour-diffusion method using the sparse-

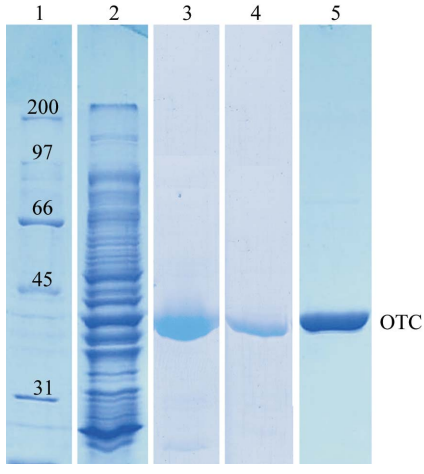

Figure 1
SDS–PAGE of cOTC samples at various steps of the purification process. Lane 1, broad-range (BioRad) molecular-weight markers (kDa); lane 2, soluble fraction from *E. coli* JM109(DE3) cells carrying the plasmid pURI3-OTC after cell disruption; lane 3, pooled fractions containing cOTC eluted from the His-Trap FF nickel-affinity column; lane 4, pooled fractions containing cOTC eluted from the HiTrap Q HP column; lane 5, pooled fractions containing cOTC eluted from Superdex 200.

matrix design (Jancarik & Kim, 1991) with Crystal Screen I (Hampton Research). Each drop contained 1 µl protein solution (24 mg ml^{-1}) in Tris–HCl buffer (10 m*M* Tris–HCl pH 8.0 containing 100 m*M* NaCl) and 1 µl reservoir solution. Drops were equilibrated against 500 µl reservoir solution. Similar procedures were used in the optimization process. Small crystals were obtained in conditions 1 and 37 of Crystal Screen I (Hampton Research), which contained 30%(*v*/*v*) 2-methyl-2,4-pentanediol, 100 m*M* sodium acetate pH 4.6, 0.02 *M* calcium chloride and 8%(*w*/*v*) PEG 4000, 100 m*M* sodium acetate pH 4.6, respectively. As a first optimization step, we used the PEG 4000-based JBScreen Classic 2 and the MPD-based JBScreen Classic 7 (Jena Bioscience). In the first case, three-dimensional small plates were obtained in condition A3, containing 8%(*w*/*v*) PEG 4000, 100 m*M* sodium acetate pH 4.6 (drops contained 1 µl protein solution and 1 µl reservoir solution). After systematic variation of buffer composition and concentration and also protein:precipitant volume ratios, crystals for diffraction experiments (0.2–0.3 mm longest dimension) were finally prepared in 8%(*w*/*v*) PEG 4000, 75 m*M* sodium acetate pH 4.6 (4 µl protein solution and 4 µl reservoir solution) (Fig. 2*a*). Crystals obtained with the JBScreen Classic 7 (Jena Bioscience) grew from conditions B5 [30%(*v*/*v*) 2-methyl-2,4-pentanediol, 100 m*M* sodium acetate pH 4.6, 0.02 *M* calcium chloride] and C4 [30%(*v*/*v*) 2-methyl-2,4-pentanediol, 5%(*w*/*v*) PEG 4000, 100 m*M* HEPES pH 7.5]. Final optimized conditions were 20%(*v*/*v*) 2-methyl-2,4-pentanediol, 7.5%(*w*/*v*) PEG 4000, 100 m*M* HEPES pH 7.8 (drops consisted of 4 µl protein solution and 4 µl reservoir solution). In this case, these conditions were reached after systematic variation of precipitant concentration and protein: precipitant volume ratios. Under these conditions, three-dimensional crystals (0.3–0.4 mm longest dimension) grew in 2 d (Fig. 2*b*).

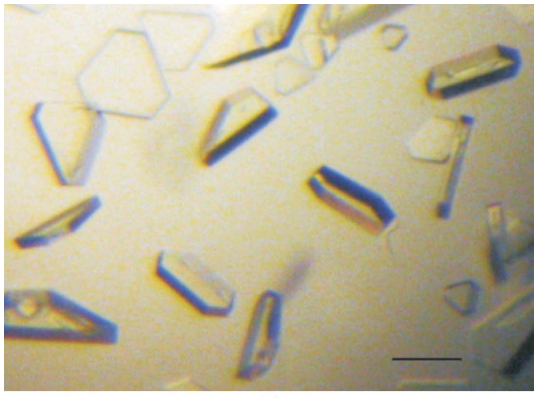

(*a*)

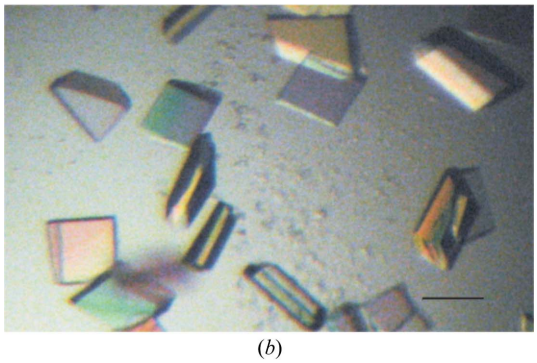

(*b*)

Figure 2
Crystals of recombinant cOTC from *L. hilgardii* grown at 291 K in (*a*) 8%(*w*/*v*) PEG 4000, 75 m*M* sodium acetate pH 4.6 and (*b*) 20%(*v*/*v*) 2-methyl-2,4-pentanediol, 7.5%(*w*/*v*) PEG 4000, 100 m*M* HEPES pH 7.8. The bar indicates 0.1 mm.

Table 1
Data-collection and processing statistics.

Values in parentheses are for the outermost shell.

	Crystal form *A*	Crystal form *B*
Space group	*P*321	*C*2
Unit-cell parameters		
a (Å)	157.04	80.06
b (Å)	157.04	148.90
c (Å)	79.28	91.67
β (°)		100.25
V_M (Å^3 Da^{-1})	2.36	2.24
Solvent content (%)	48	45
Resolution range (Å)	23.75–3.00 (3.16–3.00)	45.16–2.91 (3.01–2.91)
No. of measured reflections	68091	134717
No. of unique reflections	22713 (3121)	22503 (1960)
Completeness (%)	92.2 (91.0)	98.2 (85.9)
Multiplicity	2.8 (2.6)	6.0 (3.0)
$I > 3\sigma(I)$ (%)	73.1 (34.2)	74.6 (35.7)
$R_{\rm merge}(I)$† (%)	16.6 (35.2)	13.1 (34.7)

† $R_{\rm merge}(I) = \sum_{\mathbf{h}} \sum_l |I_{\mathbf{h}l} - \langle I_{\mathbf{h}} \rangle| / \sum_{\mathbf{h}} \sum_l \langle I_{\mathbf{h}} \rangle$, where $I_{\mathbf{h}l}$ is the lth observation of reflection **h** and $\langle I_{\mathbf{h}} \rangle$ is the weighted average intensity for all observations l of reflection **h**.

2.4. X-ray diffraction analysis and processing

For X-ray diffraction measurements at 120 K, the crystals obtained in 8%(*w*/*v*) PEG 4000, 75 m*M* sodium acetate pH 4.6 were cryoprotected by a quick soak (~10 s) in optimized reservoir solution containing 20%(*v*/*v*) 2-methyl-2,4-pentanediol and immediately flash-cooled in a stream of liquid nitrogen controlled by a Cryostream Controller 700 (Oxford Cryosystems). Crystals prepared in 20%(*v*/*v*) 2-methyl-2,4-pentanediol, 7.5%(*w*/*v*) PEG 4000, 100 m*M* HEPES pH 7.8 were directly flash-cooled. Diffraction data were collected in-house at 120 K on a Kappa 2000 Brüker–Nonius CCD detector using Cu *Kα* X-rays generated by a FR591 Brüker–Nonius rotating-anode generator equipped with a double-mirror focusing system and operated at 45 kV and 100 mA. The crystal-to-detector distance was kept at 150 mm in both cases. The images were processed and scaled using *DENZO* and *SCALEPACK* from the *HKL*-2000 suite (Otwinowski & Minor, 1997). Intensities were converted to structure-factor amplitudes using *TRUNCATE* (Collaborative Computational Project, Number 4, 1994). Data-collection statistics are given in Table 1.

The self-rotation function was calculated with *MOLREP* (Vagin & Teplyakov, 1997) from the *CCP*4 program suite (Collaborative Computational Project, Number 4, 1994) using data between 15 and 3 Å resolution and an integration radius of 30 Å. The crystal structure of cOTC was determined by the molecular-replacement method, also using *MOLREP*. The atomic coordinates of catabolic ornithine transcarbamylase from *P. aeruginosa* (PDB code 1dxh; 52% amino-acid sequence identity) were used as the search model. Refinement is currently under way using *REFMAC*5 from the *CCP*4 program suite (Collaborative Computational Project, Number 4, 1994).

3. Results and discussion

The *arcB* gene from *L. hilgardii* CECT 4786^T (ATCC 8290^T) has been cloned and the protein overexpressed in *E. coli* JM109(DE3) (pLysS) cells. Biochemical characterization of the His_6-tagged cOTC, carried out as described previously (Zúñiga *et al.*, 1998; Arena *et al.*, 2002), revealed that this recombinant protein is fully active (data not shown).

The recombinant protein behaves in solution as a chromatographically homogeneous species with a molecular weight corresponding to a hexamer (~240 kDa), as can be deduced from gel-

Table 2
Details of the molecular-replacement solutions for crystal forms *A* and *B*.

The resolution range used for rotation function and translation was 15.0–3.0 Å.

	Eulerian angles (°)			Translations (fractional)				
Subunits	α	β	γ	T_x	T_y	T_z	R	Corr
Molecular-replacement solution for crystal form *A*								
1	164.25	101.56	169.77	−0.228	−0.411	−0.179	59.8	24.4
2	76.77	−100.14	102.08	−0.147	−0.552	0.193	57.7	30.5
3	25.03	−14.84	−130.14	−0.126	−0.279	0.294	55.6	36.0
Molecular-replacement solution for crystal form *B*								
1	242.99	66.43	323.67	0.285	0.000	0.239	50.2	30.1
2	0.00	75.99	−30.25	−0.208	−0.087	0.289	45.0	44.1
3	118.33	66.68	−24.15	0.177	−0.279	0.250	39.9	56.2

filtration experiments on Superdex 200 (data not shown). Crystallization of cOTC from *L. hilgardii* was carried out by the hanging-drop vapour-diffusion method. Crystals of cOTC suitable for diffraction studies have been obtained under two experimental conditions: (i) 8%(*w*/*v*) PEG 4000, 75 m*M* sodium acetate pH 4.6 and (ii) 20%(*v*/*v*) 2-methyl-2,4-pentanediol, 7.5%(*w*/*v*) PEG 4000, 100 m*M* HEPES pH 7.8. In both cases, the final optimized drops were made up of 4 µl protein solution at 10 mg ml^{-1} and 4 µl precipitant solution. Crystals prepared under the first (acidic) conditions (crystal form *A*) belonged to the trigonal space group *P*321, with unit-cell parameters $a = b = 157.04$, $c = 79.28$ Å, and had a unit-cell volume of 1 692 363 Å^3. Conversely, crystals obtained under the second (almost neutral) conditions (crystal form *B*) belonged to the monoclinic space group *C*2 and have unit-cell parameters $a = 80.06$, $b = 148.90$, $c = 91.67$ Å, $\beta = 100.25^\circ$ and a unit-cell volume of 1 075 521 Å^3. The programs *DENZO* and *SCALEPACK* from the *HKL*-2000 suite (Otwinowski & Minor, 1997) were used for integration and scaling of the data. The completeness of the trigonal and monoclinic data was 92.2 and 98.2% (91.0 and 85.9% in the outer shell), respectively, with the $R_{\rm merge}$ values being 16.6 and 13.1% (35.2 and 34.7% in the outer shell), respectively. The number of molecules in the asymmetric unit was estimated using the Matthews probability calculator, with the resolution as an additional parameter (Kantardjieff & Rupp, 2003). The highest probabilities for both crystal forms (form *A*, 0.85; form *B*, 0.80) were obtained with three molecules in the asymmetric unit, resulting in Matthews coefficients ($V_{\rm M}$; Matthews, 1968) and solvent contents of 2.36 and 2.24 Å^3 Da^{-1} and of 48% and 45% for crystal forms *A* and *B*, respectively. Data-collection and processing statistics are shown in Table 1. Further evidence pointing to this result was obtained from analysis of the local symmetry using *MOLREP*. The self-rotation function calculated using the trigonal data revealed peaks at $\chi = 120^\circ$, showing the existence of a local threefold axis at $(\theta, \varphi, \chi) = (70, 90, 120^\circ)$ (Fig. 3*a*). On the other hand, similar analyses using the monoclinic data also showed peaks on the $\chi = 120^\circ$ section which are consistent with a local threefold axis at $(\theta, \varphi, \chi) = (6, 0, 120^\circ)$ (Fig. 3*b*). Peak intensities with respect to the crystallographic axis were 68.3% (Rf/σ = 9.37) and 80.5% (Rf/σ = 16.74), respectively. Remarkably, it can be concluded from this analysis that the noncrystallographic threefold axis is perpendicular to the twofold crystallographic axis in both crystal forms.

The structure of the catabolic ornithine transcarbamylase from *L. hilgardii* has been determined by the molecular-replacement method using the atomic coordinates of ornithine transcarbamylase from *P. aeruginosa* (Villeret *et al.*, 1995; 335 residues; PDB code 1dxh) as the search model. This model was initially chosen because cOTC from *P. aeruginosa* is the OTC of known structure that exhibits the highest sequence identity to cOTC from *L. hilgardii* (52%). Details of the molecular-replacement solutions are shown in Table 2.

The asymmetric units of both crystal forms, *A* and *B*, are made up of three identically associated cOTC polypeptide chains related by a local threefold axis, forming a trimeric structure (Fig. 4*a*). This result fully agrees with the estimated $V_{\rm M}$ values and the analysis of the local symmetry. Additionally, and identically in both crystal forms, two trimeric structures associate forming a hexamer which is endowed with 32 point-group symmetry (Fig. 4*b*). Thus, the hexamer can be described as a dimer of trimers. According to this result, cOTC from *L. hilgardii* would represent a new oligomerization state within the OTCases, which are mostly homotrimeric (Ha *et al.*, 1997; Jin *et al.*, 1997) and also dodecameric (Villeret *et al.*, 1995, 1998). In this regard,

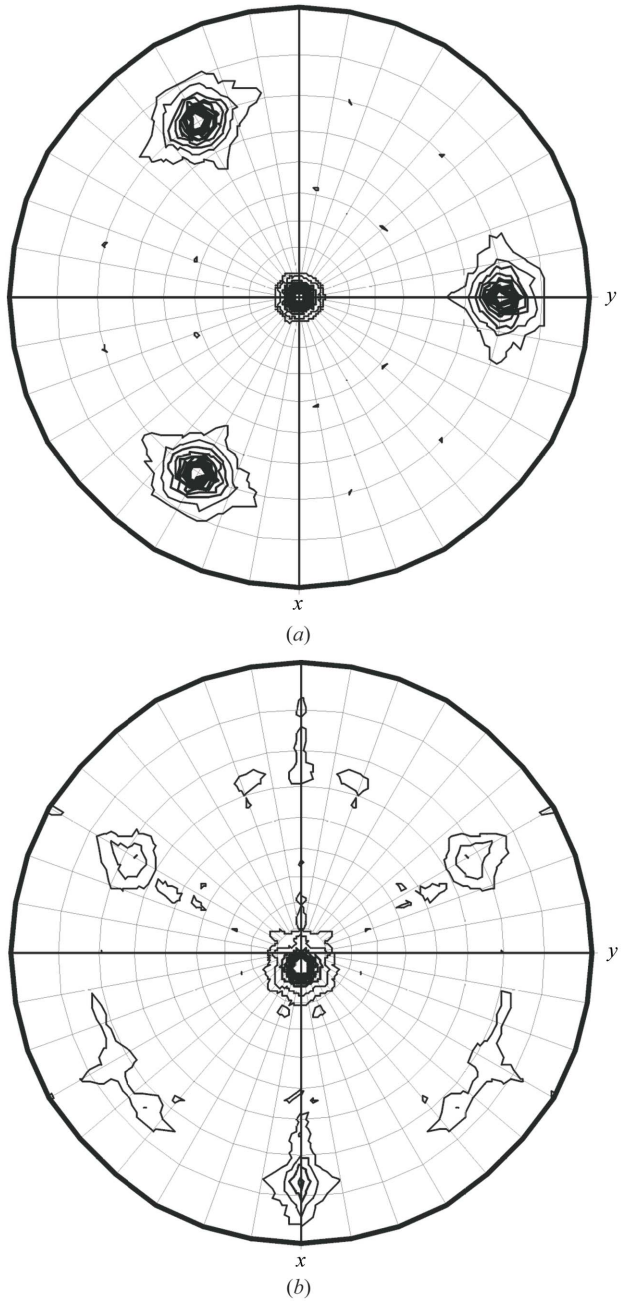

Figure 3
Projection map of the self-rotation function at the $\chi = 120^\circ$ section for (*a*) trigonal and (*b*) monoclinic data. Strong signals arising from threefold noncrystallographic symmetry are observed at $\theta = 70$, $\varphi = 90^\circ$ in (*a*) and at $\theta = 6$, $\varphi = 0^\circ$ in (*b*). The radius of integration was 30 Å and the resolution range used was 15–3 Å. The plot was generated with *MOLREP*.

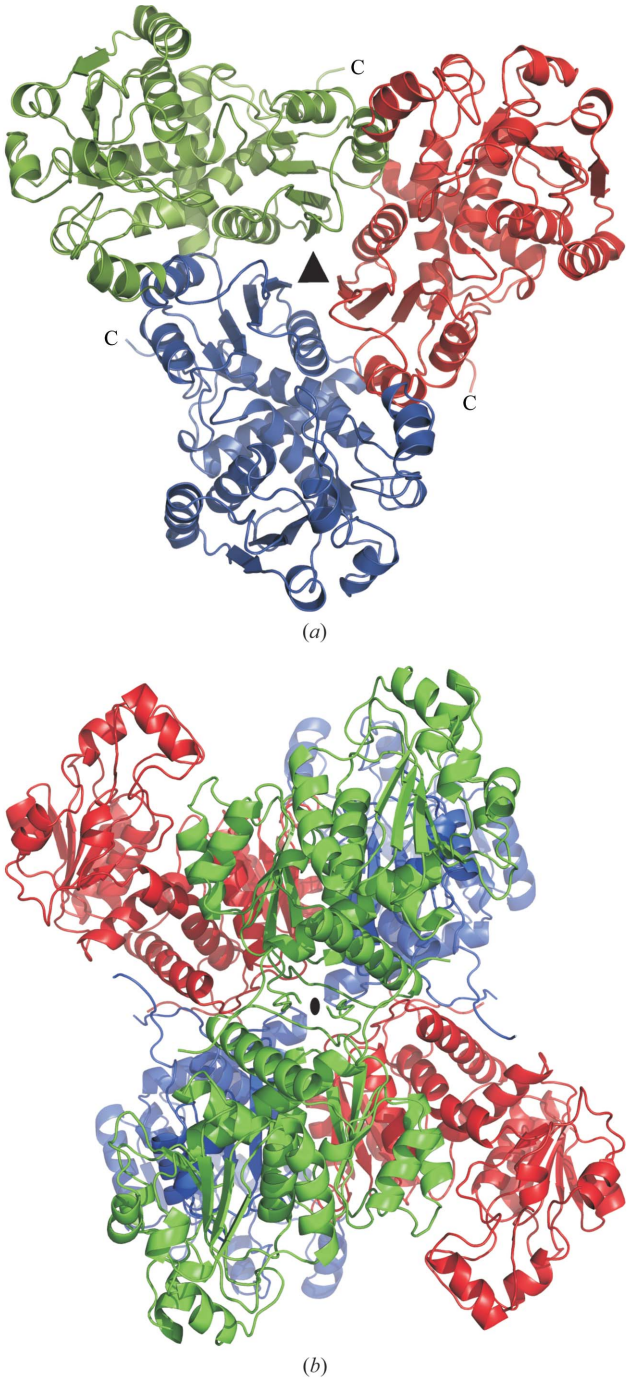

Figure 4
Asymmetric unit of the cOTC trigonal crystal and hexameric structure of cOTC. (*a*) Three molecules of cOTC (shown as ribbon models) make up the asymmetric unit of the cOTC trigonal crystals. The three polypeptide chains are related by a local threefold axis (filled triangle). Identical trimeric assemblies are present in the asymmetric unit of the cOTC monoclinic crystal. (*b*) Hexameric structure of cOTC. The twofold crystallographic axis is indicated by a filled oval. This figure was prepared using *PyMOL* (DeLano, 2002).

it is worth mentioning that the dodecameric structures of cOTC from *P. aeruginosa* (Villeret *et al.*, 1995) and anabolic OTC from *P. furiosus* (Villeret *et al.*, 1998) can be described as tetramers of trimers and thus there are no equivalent hexamers to those described here. Although the physiological oligomeric state of cOTC of *L. hilgardii* is not known, it is obvious that the results presented in this work strongly indicate that the hexamer is the native functional state. The structure refinement of cOTC is currently in progress.

JMM thanks the Ministerio de Educación y Ciencia for a research grant (BFU2004-01554/BMC; DGCYT) and 'Factoría de Cristalización' Consolider-Ingenio 2010 for support of his research and also Dr Juliana Sanz for her helpful discussions. This work was also supported by grants AGL2005-00470 (CICYT) and S-0505/AGR000153 (CAM). HR is a recipient of a I3P predoctoral fellowship from the CSIC.

References

Arena, M. E., Manca de Nadra, M. C. & Muñoz, R. (2002). *Gene*, **301**, 61–66.
Arena, M. E., Saguir, F. M. & Manca de Nadra, M. C. (1999). *Int. J. Food Microbiol.* **52**, 155–161.
Canas, B. J., Joe, F. L., Diachenko, G. W. Jr & Burns, G. (1994). *J. AOAC Int.* **77**, 1530–1536.
Collaborative Computational Project, Number 4 (1994). *Acta Cryst.* D**50**, 760–763.
Davis, C. R., Wibowo, D., Eschenbruch, R., Lee, T. H. & Fleet, G. H. (1985). *Am. J. Enol. Vitic.* **36**, 290–301.
DeLano, W. L. (2002). *PyMOL.* http://www.pymol.org.
Geiser, M., Cèbe, R., Drewello, D. & Schemitz, R. (2001). *Biotechniques*, **31**, 88–92.
Ha, Y., McCann, M. T., Tuchman, M. & Allewell, N. M. (1997). *Proc. Natl Acad. Sci. USA*, **94**, 9550–9555.
Jancarik, J. & Kim, S.-H. (1991). *J. Appl. Cryst.* **24**, 409–411.
Jin, L., Seaton, B. A. & Head, J. F. (1997). *Nature Struct. Biol.* **4**, 622–625.
Kantardjieff, K. A. & Rupp, B. (2003). *Protein Sci.* **12**, 1865–1871.
Lipscomb, W. N. (1994). *Adv. Enzymol. Relat. Areas Mol. Biol.* **68**, 67–151.
Lehtonen, P. (1996). *Am. J. Enol. Vitic.* **47**, 127–133.
Liu, S.-Q. & Pilone, G. J. (1998). *J. Appl. Microbiol.* **84**, 315–327.
Liu, S.-Q., Pritchard, G. G., Hardman, M. J. & Pilone, G. J. (1995). *Appl. Environ. Microbiol.* **61**, 310–316.
Massant, J., Wouters, J. & Glansdorff, N. (2003). *Acta Cryst.* D**59**, 2140–2149.
Matthews, B. W. (1968). *J. Mol. Biol.* **33**, 491–497.
Mirvish, S. S. (1968). *Adv. Cancer Res.* **11**, 1–42.
Monteiro, F. F. & Bisson, L. F. (1991). *Am. J. Enol. Vitic.* **42**, 199–208.
Otwinowski, Z. & Minor, W. (1997). *Methods Enzymol.* **276**, 307–326.
Ough, C. S. (1993). *Bull. Soc. Med. Friends Wine*, **25**, 7–8.
Ough, C. S., Crowell, E. A. & Gutlove, B. R. (1998). *Am. J. Enol. Vitic.* **39**, 239–242.
Shi, D., Morizono, M., Ha, Y., Aoyagi, M., Tuchman, M. & Allewell, N. M. (1998). *J. Biol. Chem.* **273**, 34247–34254.
Spayd, S. E. & Andersen-Bagge, J. (1996). *Am. J. Enol. Vitic.* **47**, 389–402.
Sponholz, W. R. (1991). *Proceedings of the International Symposium on Nitrogen in Grapes and Wine*, edited by J. M. Rantz, pp. 67–77. California: American Society for Enology and Viticulture.
Sponholz, W. R. (1992). *Biol. Oggi*, **6**, 15–24.
Tuchman, M., Morizono, H., Reish, O., Yuan, X. & Allewell, N. M. (1995). *J. Med. Genet.* **32**, 680–688.
Vagin, A. & Teplyakov, A. (1997). *J. Appl. Cryst.* **30**, 1022–1025.
Villeret, V., Clantin, B., Tricot, C., Legrain, C., Roovers, M., Stalon, V., Glansdorff, N. & Dideberg, O. (1998). *Proc. Natl Acad. Sci. USA*, **95**, 2801–2806.
Villeret, V., Tricot, C., Stalon, V. & Dideberg, O. (1995). *Proc. Natl Acad. Sci. USA*, **92**, 10762–10766.
Zúñiga, M., Champomier-Verges, M., Zagorec, M. & Pérez-Martínez, G. (1998). *J. Bacteriol.* **180**, 4154–4159.